NJC

RSC Publishing

PAPER

View Article Online
View Journal

Cite this: DOI: 10.1039/c3nj00542a

Studies of ruthenium(II)-2,2′-bisimidazole complexes on binding to G-quadruplex DNA and inducing apoptosis in HeLa cells†

Yu Xia, Qingchang Chen, Xiuying Qin, Dongdong Sun, Jingnan Zhang and Jie Liu*

Received (in Montpellier, France)
22nd May 2013,
Accepted 21st August 2013

DOI: 10.1039/c3nj00542a

www.rsc.org/njc

Three ruthenium(II) complexes $[Ru(bpy)_2(biim)]^{2+}$ (**1**), $[Ru(phen)_2(biim)]^{2+}$ (**2**) and $[Ru(p\text{-mopip})_2\text{-}(biim)]^{2+}$ (**3**) (where bpy is 2,2′-bipyridine, phen is 1,10-phenanthroline, biim is 2,2′-bisimidazole and *p*-mopip is 2-(4-methoxyphenyl)-imidazo-[4,5*f*]phenanthroline), have been synthesized and characterized. The interactions of human telomeric DNA oligomers 5′-$G_3(T_2AG_3)_3$-3′ (HTG21) with ruthenium(II) complexes were investigated *via* UV-vis, fluorescence resonance energy transfer (FRET) melting assay, polymerase chain reaction (PCR) stop assay, and circular dichroism (CD) measurements. The results indicated that the three ruthenium(II) complexes could stabilize the formation of human telomeric G-quadruplex DNA, and complex **2** was found to be the most efficient. *In vitro* cytotoxicity assay by MTT also showed that complex **2** was superior to complexes **1** and **3** in inhibiting the growth of cancer cells. Telomeric repeat amplification protocol (TRAP) showed that complexes **2** and **3** led to an inhibition of the telomerase activity, and complex **2** was the significantly better inhibitor. Flow cytometric analysis and evaluation of mitochondrial membrane potential demonstrated that complex **2** inhibited the growth of HeLa cells through induction of apoptotic cell death, as evidenced by the depletion of mitochondrial membrane potential in HeLa cells.

1 Introduction

The human telomeric DNA consists of the tandem repeat sequence $[TTAGGGCCCTAA]_n$. Several kilobases of this sequence are paired with a complementary strand to form duplex DNA, but about two hundred bases are unpaired as a single-stranded overhang.[1] This single G-rich strand has the inclination to adopt higher-order and functionally useful four-stranded structures called G-quadruplexes.[2] Recent studies suggest that the G-quadruplex structures exist *in vivo*[3] and such structures form in telomeric DNA at specific times during the cell cycle.[4] It has been shown that the stabilization of G-quadruplexes can effectively inhibit telomerase activity which is expressed in over 85% of tumor cell lines but in relatively few normal cell types[5] and ultimately alter telomere maintenance.[6,7] Telomere maintenance is very significant for the unlimited proliferative potential of cancer cells.[8] Consequently, the inhibition of telomerase activity by inducing G-quadruplex formation is very important for developing new anticancer drugs.[9]

A number of small molecules have been reported to efficiently stabilize G-quadruplex DNA, and recently some metal complexes as G-quadruplex DNA stabilizers were reported.[10–14] The metal can play a major structural role in organizing the ligands into an optimal structure for G-quadruplex DNA interaction. It is likely that such stabilization occurs due to π–π interactions between the large aromatic ligands of the ruthenium(II) complexes and DNA guanine residues. Ruthenium(II) complexes have prominent DNA binding properties.[15] For example, the typical ruthenium complex $[Ru(bpy)_2(dppz)]^{2+}$ (dppz = dipyrido[3,2-*a*:2′,3′-*c*]phenazine) is known as DNA "light switch".[16,17] Such complexes can tightly intercalate between the duplex DNA base pairs and stabilize the DNA.[18] Some of them have been studied as synthetic restriction enzymes, nucleic acid probes, anticancer drugs, and DNA footprinting agents, *etc.*[19–21] Rickling *et al.* studied the action of the dinuclear $[(tap)_2Ru(tpac)Ru(tap)_2]^{4+}$ complex (tapc = tetrapyridoacridine) with the $[TTAGGG]_4$ sequence. They found that the complex damaged the sequences by photobridging intramolecularly two or more G bases with the metallic $[(tap)_2\text{-}Ru(tpac)Ru(tap)_2]^{4+}$. The photoinduced bridging process "froze" the folded G-quadruplex conformation.[22] Thomas *et al.* reported that the dinuclear tppz-based systems could bind with high affinity to quadruplex DNA at high ionic strengths through the 22-mer $d(AG_3[T_2AG_3]_3)[G_3]$ human telomeric sequence.[23] The international community has widely recognized that some

Department of Chemistry, Jinan University, Guangzhou 510632, P. R. China. E-mail: tliuliu@jnu.edu.cn; Fax: +86-20-8522-1263

† Electronic supplementary information (ESI) available: ESI-MS and ^1H NMR spectra of complexes **1**, **2** and **3** (Fig. S1, S2 and S3). Absorbance spectra (λ_{max}/nm) and DNA-binding constants K_b ($\times 10^6$ M^{-1}) of complexes **1**, **2** and **3**. See DOI: 10.1039/c3nj00542a

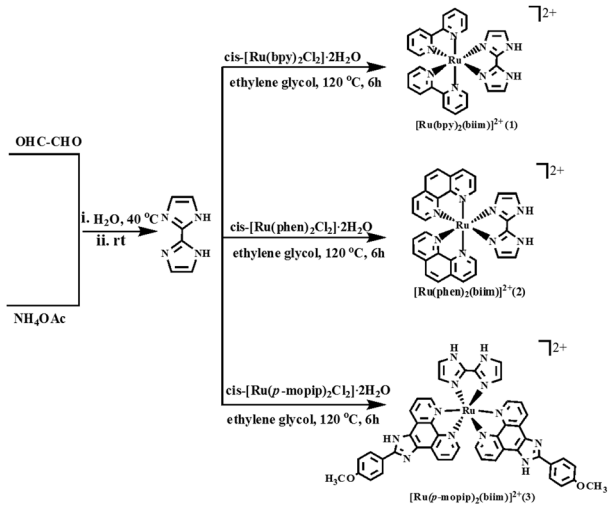

Scheme 1 Synthetic routes for the preparation of complexes **1**, **2** and **3**.

ruthenium complexes exhibit great cytotoxicity toward cancer cells but low toxicity to normal cells, they are easily absorbed by tumor tissue and rapidly excreted from the body.[24,25]

It is very inspiring that the promising ruthenium anticancer agents, [ImH][*trans*-$RuCl_4$(Im)(DMSO)] (NAMI-A, where DMSO = dimethyl sulfoxide and Im = imidazole), [IndH][*trans*-$RuCl_4(Ind)_2$] (KP1019, where Ind = indazole) and *trans*-[$RuCl_4(Ind)_2$]IndH (NKP-1339),[26–28] have successfully entered clinical trials. These reports make ruthenium complexes containing imidazole and their derivative ligands draw much attention.[29,30] In the past few years, our group has been committed to the research on antitumor properties of ruthenium complexes including their design, synthesis, structural modification, biological activity and mechanisms.[31] In our previous studies, we found that ruthenium complexes containing methylimidazole ligands, such as $[Ru(MeIm)_4(N–N)]^{2+}$ [N–N = tip, iip, dppz, dpq], had some antitumor activity. We designed three new complexes $[Ru(bpy)_2(biim)]^{2+}$ (**1**), $[Ru(phen)_2(biim)]^{2+}$ (**2**) and $[Ru(p\text{-mopip})_2(biim)]^{2+}$ (**3**), all the three complexes have bisimidazole as the main ligand (Scheme 1). It was well known that the H linking to the N atom of bisimidazole may form hydrogen-bonding with the functional groups located on the edges of DNA to favor interaction of the main ligand, and thus such a ligand strengthens the DNA-binding affinity of the complex.[32] The interaction of human telomeric G-quadruplex DNA with the three complexes has been studied. Importantly, complex **2** exhibited potent antitumor activities and effectively inhibited telomerase activity. The biological properties of complex **2**, the most active ruthenium complex among the three, were studied by showing its apoptosis-inducing activities and related signaling pathways in HeLa tumor cells.

2 Experimental

2.1 Reagents and materials

All the reagents and solvents were purchased from commercial sources and used without further purification. Human telomeric DNA oligomers HTG21 were purchased from Shanghai Sangon Biological Engineering Technology & Services (Shanghai, China) and used without further purification. The concentration of HTG21 was determined by measuring the absorbance at 260 nm after melting. Single-strand molar absorptivities were calculated from mononucleotide data using a nearest-neighbour approximation. The formation of intramolecular G-quadruplexes was carried out as follows: the oligonucleotide samples, dissolved in different buffers, were heated to 90 °C for 5 min, gently cooled to room temperature, and then incubated at 4 °C overnight. Buffer: 10 mM Tris-HCl, pH = 7.4. Solutions of DNA in 5 mM Tris-HCl/50 mM NaCl buffer in water gave a ratio of UV absorbance at 260 and 280 nm, A_{260}/A_{280}, of 1.9. The concentration of DNA in nucleotide phosphate (NP) was determined by UV absorbance at 260 nm after 1 : 100 dilution. The molar absorptivity, ε_{260}, was determined to be 6600 M^{-1} cm^{-1}. Stock solutions were stored at 4 °C and used after no more than 4 days.

2.2 Physical measurements

Microanalysis (C, H and N) was carried out using a Perkin-Elmer 240C elemental analyzer. Electrospray ionization mass spectrometry (ESI-MS) was performed on a LQC system (Finngan MAT, USA) using CH_3CN as the mobile phase. ^{1}H NMR spectra were recorded on a Varian Mercury-plus 300 NMR spectrometer with d_6-DMSO as the solvent and $SiMe_4$ as an internal standard at 300 MHz at room temperature. All chemical shifts were given relative to TMS (tetramethylsilane). UV-Vis spectra were measured on a Perkin-Elmer Lambda-850 spectrophotometer. Circular dichroism (CD) spectra were recorded on a Jasco J-810 spectropolarimeter.

2.3 Synthesis and characteristics

Ruthenium(III) chloride hydrate (Alfa Aesar), ethanedial (Sigma), 1,10-phenanthroline (Sigma), and 4-methoxybenzaldehyde (Sigma) were used. The compounds 2,2′-bisimidazole, 1,10-phenanthroline-5,6-dione, *p*-mopip and *cis*-[$Ru(bpy)_2Cl_2$]·$2H_2O$ and *cis*-[$Ru(phen)_2Cl_2$]·$2H_2O$ were prepared and characterized according to methods described in the literature.[33–35]

2.3.1 Synthesis of *cis*-[$Ru(bpy)_2(biim)](PF_6)_2$. A mixture of *cis*-[$Ru(bpy)_2Cl_2$]·$2H_2O$ (0.26 g, 0.5 mmol), biim (0.067 g, 0.5 mmol), and ethylene glycol (20 mL) was refluxed for 6 h under argon. The cooled reaction mixture was diluted with water (50 mL). Saturated aqueous sodium hexafluorophosphate solution was added under vigorous stirring, and filtered. The dark red solid was collected and washed with small amounts of water, and diethyl ether, then dried under vacuum, and purified by column chromatography on alumina using acetonitrile–toluene (12 : 1 v/v) as the eluant. The solvent was removed under reduced pressure and red microcrystals were obtained (0.25 g, 60% yield). ^{1}H NMR (300 MHz, [D_6]DMSO, 25 °C): δ 8.75 (d, J = 7.8 Hz, 4H, bpy-H_6, $H_{6'}$), 8.11 (t, J_1 = 7.5 Hz, J_2 = 6.9 Hz, 4H, bpy-H_3, $H_{3'}$), 7.84 (d, J = 6.5 Hz, 4H, bpy-H_4, $H_{4'}$), 7.46 (t, J = 6.5 Hz, 4H, bpy-H_5, $H_{5'}$), 7.56 (d, J = 6.2 Hz, 2H, biim-H_5, $H_{5'}$), 6.44 (d, J = 6.3 Hz, 2H, biim-H_4, $H_{4'}$). MS (ESI^+, CH_3CN): m/z = 547.1 $[M]^+$ (see Fig. S1, ESI†). $C_{26}H_{22}N_8Ru$ (547.58): calcd C 37.29, H 2.65, N 13.38%; found C 37.27, H 2.66, N 13.35%.

2.3.2 Synthesis of *cis*-[Ru(phen)$_2$(biim)](PF$_6$)$_2$. A mixture of *cis*-[Ru(phen)$_2$Cl$_2$]·2H$_2$O (0.284 g, 0.5 mmol), biim (0.067 g, 0.5 mmol), and ethylene glycol (20 mL) was refluxed for 6 h under argon. The cooled reaction mixture was diluted with water (50 mL). Saturated aqueous sodium hexafluorophosphate solution was added under vigorous stirring, and filtered. The dark red solid was collected and washed with small amounts of water, and diethyl ether, then dried under vacuum, and purified by column chromatography on alumina using acetonitrile–toluene (13 : 1 v/v) as the eluant. The solvent was removed under reduced pressure and red microcrystals were obtained (0.22 g, 49% yield). ^{1}H NMR (300 MHz, [D$_6$]DMSO, 25 °C): δ 8.79 (d, J = 7.7 Hz, 2H, phen-H$_2$), 8.66 (d, J = 8.3 Hz, 2H, phen-H$_9$), 8.35 (m, J_1 = 7.2 Hz, J_2 = 5.5 Hz, 6H, phen-H$_4$, H$_7$, H$_5$), 8.11 (d, J = 6.7 Hz, 2H, phen-H$_6$), 8.01 (d, J = 7.9 Hz, 2H, phen-H$_8$), 7.43 (d, J = 7.1 Hz, 2H, phen-H$_3$), 7.68 (d, J = 6.2 Hz, 2H, biim-H$_5$, H$_{5'}$), 6.39 (d, J = 5.6 Hz, 2H, biim-H$_4$, H$_{4'}$). MS (ESI$^+$, CH$_3$CN): m/z = 595.2 [M]$^+$ (see Fig. S2, ESI†). C$_{30}$H$_{22}$N$_8$Ru (595.62): calcd C 40.69, H 2.50, N 12.65%; found C 40.65, H 2.52, N 12.61%.

2.3.3 Synthesis of *cis*-[Ru(*p*-mopip)$_2$(biim)](PF$_6$)$_2$. A mixture of *cis*-[Ru(*p*-mopip)$_2$Cl$_2$]·2H$_2$O (0.43 g, 0.5 mmol), biim (0.067 g, 0.5 mmol), and ethylene glycol (20 mL) was refluxed for 6 h under argon. The cooled reaction mixture was diluted with water (50 mL). Saturated aqueous sodium hexafluorophosphate solution was added under vigorous stirring, and filtered. The dark red solid was collected and washed with small amounts of water, and diethyl ether, then dried under vacuum, and purified by column chromatography on alumina using acetonitrile–ethanol (8 : 1 v/v) as the eluant. The solvent was removed under reduced pressure and red microcrystals were obtained (0.32 g, 54% yield). ^{1}H NMR (300 MHz, [D$_6$]DMSO, 25 °C): δ 9.05 (d, J = 7.1 Hz, 4H, *p*-mopip), 8.91 (d, J = 7.8 Hz, 4H, *p*-mopip), 8.33 (m, J_1 = 8.8 Hz, J_2 = 7.2 Hz, 4H, *p*-mopip), 8.00 (d, J = 8.5 Hz, 4H, *p*-mopip), 7.81 (d, J = 8.5 Hz, 4H, *p*-mopip), 6.4–7.6 (d, J = 6.2 Hz, 4H, biim-H$_4$, H$_{4'}$, H$_5$, H$_{5'}$). MS (ESI$^+$, CH$_3$CN): m/z = 887.3 [M]$^+$ (see Fig. S3, ESI†). C$_{46}$H$_{34}$N$_{12}$O$_2$Ru (887.91): calcd C 46.91, H 2.91, N 14.27%; found C 46.95, H 2.94, N 14.22%.

2.4 Absorbance spectra

Absorbance spectra titrations were carried out at room temperature to determine the binding affinity between DNA and the complex. Initially, 3 mL water solutions of the blank buffer and the ruthenium complex sample (10 μM) dissolved in distilled water were placed in the reference and sample cuvettes (1.0 cm path length), respectively, and then the first spectrum was recorded in the range of 200–600 nm. During the titration, 1–10 μL aliquot of buffered DNA solution was added to each cuvette to eliminate the absorbance of DNA, and the solutions were mixed by repeated inversion. Complex–DNA solutions were incubated for 5 min before absorption spectra were recorded. The titration processes were repeated until there was no change in the spectra for four titrations at least, indicating that binding saturation had been achieved. The changes in the metal complex concentration due to dilution at the end of each titration were negligible.

2.5 Fluorescence resonance energy transfer (FRET)

The fluorescent labeled oligonucleotide, F21T (5′-FAM-G$_3$[T$_2$AG$_3$]$_3$-TAMRA-3′, FAM:6-carboxyfluorescein, TAMRA:6-carboxytetramethylrhodamine), used as the FRET probe was diluted in Tris-HCl buffer (10 mM, pH 7.4) containing KCl (60 mM) and then annealed by heating to 92 °C for 5 min, followed by slow cooling to room temperature, overnight. Fluorescence melting curves were determined using a Bio-Rad iQ5 real time PCR detection system, by using a total reaction volume of 20 μL, with labeled oligonucleotide (1 μM) and different concentrations of complexes in Tris-HCl buffer (10 mM, pH 7.4) containing KCl (60 mM). Fluorescence readings with an excitation wave at 470 nm and detection at 530 nm were taken at intervals of 1 °C over the range 30–95 °C, with a constant temperature being maintained for 30 s prior to each reading to ensure a stable value. The melting of the G-quadruplex was monitored alone or in the presence of various concentrations of complexes. Final analysis of the data was carried out by using Origin 6.0.

2.6 PCR stop assay

The oligonucleotide HTG21 (5′-G$_3$[T$_2$AG$_3$]$_3$-3′) and the corresponding complementary sequence (HTG21rev, ATCGCTTCTCGTCCCTAACC) were used. The reactions were performed in 1 × PCR buffer, containing each oligonucleotide (10 pmol each), dNTPs (0.16 mM), Taq polymerase (2.5 U), and different concentrations of complexes. Reaction mixtures were incubated in a thermocycler under the following cycling conditions: 94 °C for 3 min, followed by 30 cycles of 94 °C for 30 s, 58 °C for 30 s, and 72 °C for 30 s. PCR products were then analyzed on a nondenaturing polyacrylamide gel (15%) in 1 × TBE and silver stained.

2.7 Circular dichroism (CD)

CD experiments were performed on a JASCO-J810 circular dichroism spectrophotometer. A quartz cuvette with 4 mm path length was used for the spectra recorded over a wavelength range of 230–400 nm at 1 nm bandwidth, 1 nm step size, and 0.5 s time per point. The oligomer HTG21 was diluted from stock to the correct concentration (2 μM) in Tris-HCl buffer (10 mM, pH 7.4) and then annealed by heating to 90 °C for 5 min, gradually cooled to room temperature, and incubated at 4 °C overnight. Then, CD titration was performed at a fixed HTG21 concentration (2 μM) with various concentrations (2.0 mol equiv.) of the complexes in buffer at 25 °C. After each addition of the complexes, the reaction was stirred and allowed to equilibrate for at least 3 min until no elliptic changes were observed and a CD spectrum was collected. Buffer baseline was collected in the same cuvette and subtracted from the sample spectra. Final analysis of the data was carried out using Origin 6.0.

2.8 Cell culture

Cells were cultured in a RPMI 1640 medium supplemented with heat inactivated fetal bovine serum (FBS, 10%), penicillin (100 μg mL^{-1}), and streptomycin (100 μg mL^{-1}). Cells were maintained at 37 °C in a 5% CO_2 incubator, and the medium was changed twice weekly.

2.9 MTT assay

HeLa (human cervical cancer), A549 (human lung carcinoma) and HepG2 (human hepatocellular liver carcinoma) cells were grown in a RPMI 1640 medium supplemented with FBS (10%), penicillin (100 μg mL^{-1}) and streptomycin (100 μg mL^{-1}). They were incubated at 37 °C in a humidified incubator with 5% CO_2 and 95% air. Cells at the exponential growth phase were diluted to 2.5 × 10^3 cells mL^{-1} with RPMI 1640, and then seeded in 96-well culture clusters (Costar) at a volume of 100 μL per well, and incubated for 24 h at 37 °C in 5% CO_2. Then the cells were treated with various concentrations of the complex (5, 10, 25, 50, 75, 100, 150 and 200 mmol L^{-1}); the medium and drug-free control samples were prepared simultaneously. After incubation of the cells for up to 48 h, MTT (100 μL, 5 mg mL^{-1}) solution was added to each well. After a further period of incubation (4 h at 37 °C in 5% CO_2) the cell lysate (100 μL) was added to each well. After 12 h at 37 °C, the plates were analyzed on a microplate reader at a wavelength of 570 nm (the absorbance of the complexes at this wavelength can be neglected). The percent growth inhibitory rate of treated cells was calculated as $(A_{control} - A_{drug}/A_{control} - A_{cell\text{-}free}) \times 100\%$, where A is the mean value calculated by using the data from three replicate tests. The IC_{50} values were determined by plotting the percentage viability *versus* concentration on a logarithmic graph and reading the concentration at which 50% of cells were viable relative to the control.

2.10 TRAP assay

The telomerase extract was prepared from HepG-2 cells. A modified version of the TRAP assay was used in this experiment. PCR was performed in a final 50 μL reaction volume composed of a 45 μL reaction mix containing 20 mM Tris-HCl (pH 8.0), 50 μM deoxynucleotide triphosphates, 1.5 mM $MgCl_2$, 63 mM KCl, 1 mM EDTA, 0.005% Tween 20, 20 μg mL^{-1} BSA, 3.5 pmol of primer HTG21 (5′-$G_3(T_2AG_3)_3$-3′), 18 pmol of primer TS (5′-AATCCGTCGAGCAGAGTT-3′), 22.5 pmol of primer CXext (5′-GTGCCCTTACCCTTACCCTTACCCTAA-3′), 2.5 U of Taq DNA polymerase, and 100 ng of telomerase. Complexes or distilled water was added at a volume of 5 μL. PCR was performed in an Eppendorf Master cycler equipped with a hot lid and incubated for 30 min at 30 °C, followed by 92 °C 30 s, 52 °C 30 s, and 72 °C 30 s for 30 cycles. After amplification, 8 μL of loading buffer (containing 5 × Tris-Borate-EDTA buffer (TBE buffer), 0.2% bromophenol blue, and 0.2% xylene cyanol) was added to the reaction. A 15 μL aliquot was loaded onto a 10% non-denaturing acrylamide gel (19 : 1) in 1 × TBE buffer and electrophoresed at 200 V for 1 h. Gels were fixed and then stained with $AgNO_3$.

2.11 Flow cytometric analysis

The cell cycle distribution was analyzed using flow cytometry as previously described. Cells exposed to the complexes were trypsinized and washed with PBS. After adding 70% ethanol and overnight fixation at −20 °C, the trypsinized cells were stained with propidium iodide (PI) for 4 h in the dark. The DNA content was measured using a Epics XL-MCL flow cytometer (Beckman Coulter, Miami, FL) and the cell cycle distribution was analyzed by MultiCycle software (Phoenix FlowSystems, San Diego, CA). Apoptotic cells with hypodiploid DNA content were measured by quantifying the sub-G1 peak in the cell cycle pattern. Each experiment per sample was determined by recording 10 000 events.

2.12 Evaluation of mitochondrial membrane potential ($\Delta\Psi_m$)

The mitochondrial membrane potential was measured by the JC-1 (5,5′,6,6′-tetrachloro-1,1′,3,3′-tetraethylbenzimidazolylcarbocyanine iodide) probe purchased from Beyotime Institute of Biotechnology. Firstly, cells in 6-well plates were trypsinized and resuspended in 0.5 mL of PBS buffer containing 10 μg mL^{-1} of JC-1. After 10 min incubation at 37 °C in the dark, the supernatant was immediately removed by centrifugation. After being washed and resuspended in PBS, the stained cells were immediately analyzed using flow cytometry. The percentage of the green fluorescence from JC-1 monomers was used to demonstrate the cells that lost $\Delta\Psi_m$.

3 Results and discussion

3.1 DNA-binding studies by absorbance spectroscopy

Electronic absorbance spectroscopy is one of the most useful ways to investigate the interactions of complexes with DNA.[36] Complex binding to DNA usually results in hypochromism and red shift. The extent of the hypochromism and red shift parallels the binding affinity.[37] The absorbance spectra of complexes **1**, **2** and **3** in the absence and presence of HTG21 (at a constant concentration of complexes, [Ru] = 10 μM) were obtained. With the increase in concentration of HTG21, all the absorbance bands of the complexes displayed clear hypochromism. The hypochromism (H%), as defined by H% = 100% $(A_{free} - A_{bound})/A_{free}$, of MLCT bands at about 480 nm of **1**, **2** and **3** were 13%, 29% and 23% with slight red shifts, respectively (Fig. 1 and eqn (1), ESI†). Hypochromism and red shifts indicated strong interactions between the three complexes and HTG21. The intrinsic binding constants K_b of **1**, **2** and **3** were measured to be 1.15 × 10^6 M^{-1}, 2.91 × 10^7 M^{-1} and 1.5 × 10^7 M^{-1}, respectively, from the decay of the absorbance (see Table S1 and Fig. S4, ESI†). The binding constant K_b of complex **2** is larger than that of complexes **1** and **3**, which indicates that complex **2** is bound to HTG21 more tightly than complexes **1** and **3**.

3.2 The studies of thermodynamic stabilization

To evaluate the stabilization of complexes **1**, **2** and **3** for G-quadruplex F21T (sequence: 5′-FAM-$G_3[T_2AG_3]_3$-TAMRA-3′,

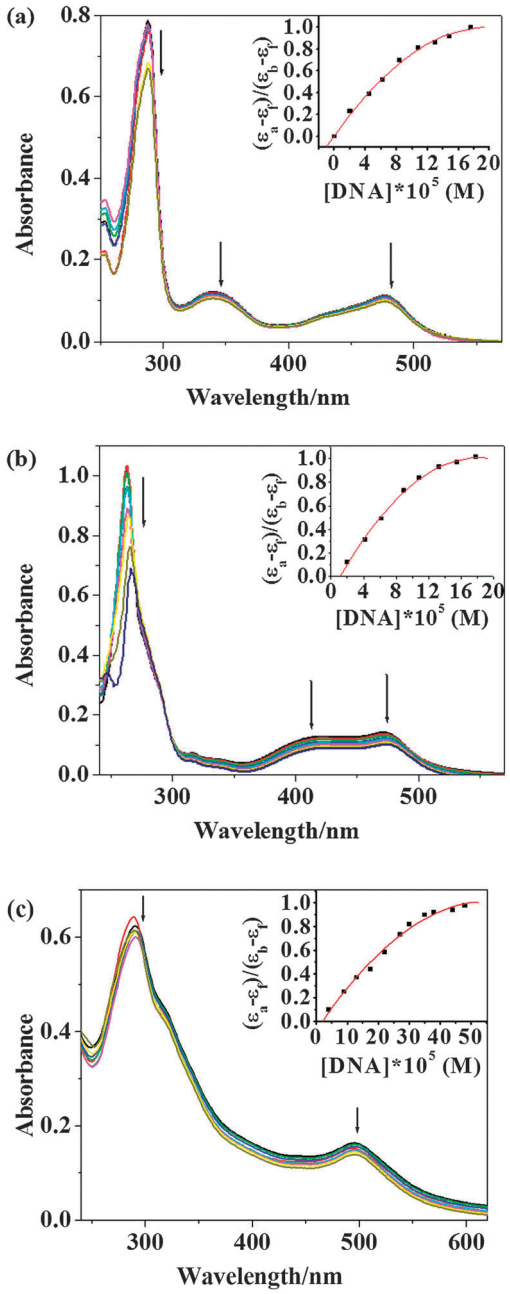

Fig. 1 Absorbance spectra of complexes **1** (a), **2** (b) and **3** (c) in buffer at 25 °C in the presence of increasing amounts of HTG21. [Ru] = 10 μM, [DNA] = 0–10 μM from top to bottom. Arrows indicate the change in absorbance upon increasing the DNA concentration.

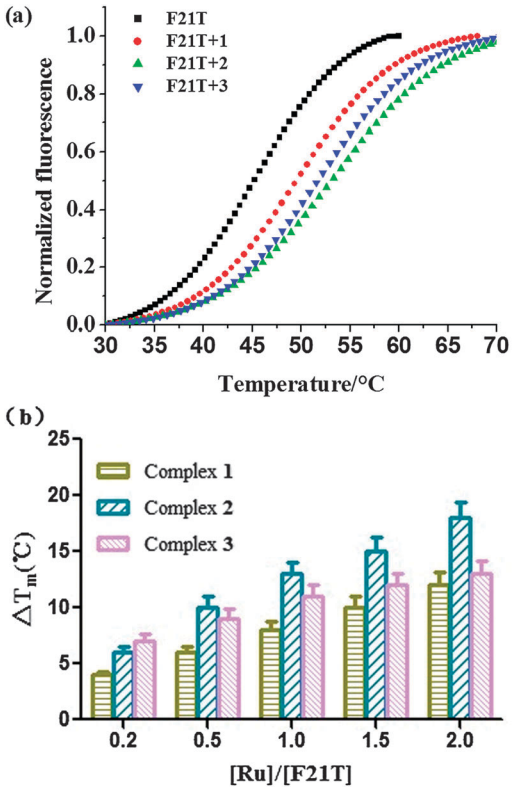

Fig. 2 (a) Melting curves of G-quadruplex F21T (1 μM) in the absence of complexes (black) and in the presence of complex **1** (red), **2** (blue) and **3** (green) at a concentration of 1 μM in Tris-HCl buffer (10 mM, pH 7.4) with 60 mM KCl. (b) DNA stabilization temperature *versus* the concentration of complexes **1**, **2** and **3** binding to F21T.

mimicking the human telomeric repeat, where FAM is the donor fluorophore 6-carboxyfluorescein and TAMRA is the acceptor 6-carboxytetramethylrhodamine), FRET melting experiments were carried out.[38] Fig. 2a shows the melting curves of G-quadruplex F21T (0.2 μM) in the presence of **1**, **2** and **3**. It was clear that **1**, **2** and **3** at a concentration of 1 μM could raise the melting temperature of the G-quadruplex by about 8 °C, 13 °C and 11 °C, respectively. Fig. 2b shows that the stabilization of G-quadruplex DNA depended on the concentration of complexes. The results demonstrated an obvious stabilization effect of these three complexes on G-quadruplex F21T. The ΔT_m value of complex **2** was the highest, indicating that complex **2** possessed a stronger stabilizing ability to the F21T G-quadruplex than complexes **1** and **3**.

3.3 Inhibition of amplification of HTG21

In order to further evaluate the ability of complexes **1**, **2** and **3** to stabilize G-quadruplex DNA, polymerase chain reaction (PCR) stop assay was carried out to ascertain whether complexes were bound to the test oligomer (5′-$G_3(T_2AG_3)_3$-3′) and stabilized the G-quadruplex structure.[39] In the presence of the complexes tested, the template sequence 5′-$G_3(T_2AG_3)_3$-3′ was induced into a G-quadruplex structure that blocked the hybridization with a complementary primer sequence. In that case, the 5′ to 3′ primer extension by DNA Taq polymerase was arrested and the final double-stranded DNA PCR product could not be detected. The inhibitory effect of **1** and **3** was gradually enhanced as the concentrations were increased from 2.5 to 15 μM with no PCR product detected at 17.5 μM (Fig. 3). Meanwhile, **2** at a concentration of 10.0 μM could completely inhibit the formation of the PCR product. The IC_{50} values of **1**, **2** and **3** were estimated to be 16.28 (±1.07), 7.45 (±0.63) and 13.14 (±0.83) μM, respectively. The PCR assay further indicated that complex **2** is a better G-quadruplex binder.

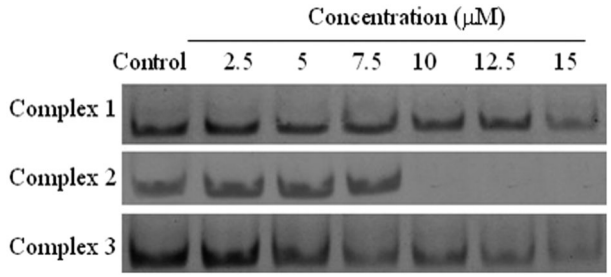

Fig. 3 Dose-dependent inhibition of HTG21 PCR amplification by complexes **1**, **2** and **3**.

3.4 Circular dichroism (CD) spectra

Circular dichroism (CD) spectroscopy can be used to monitor the formation of the G-quadruplex structure.[40] Fig. 4 displays the CD spectra for the titration of HTG21 oligonucleotide with increasing amounts of complexes. In the absence of salt, the CD spectrum of the HTG21 was found to have a major positive band at 253 nm and a positive band near 295 nm (Fig. 4a, black line), which indicates the coexistence of a single strand, parallel and antiparallel G-quadruplex.[41] Upon titration with complexes **1**, **2** and **3** into HTG21 oligonucleotide, dramatic changes in the CD spectra were observed.

As shown in Fig. 4a, the maximum at 253 nm was gradually suppressed and shifted toward 245 nm, while the band centered at about 293 nm increased dramatically with an increase in the concentration of **1**. Meanwhile, a major negative band at about 261 nm started to appear. The CD spectrum of this new DNA conformation was virtually consistent with the CD spectra of antiparallel G-quadruplexes described in previous studies, where the major positive band was usually observed around 290 nm with a negative band at 265 nm and a smaller positive band at 246 nm.[42] As the concentration of **1** further increased to 7 μM, a strong shoulder located near 275 nm as the spectral characteristic of a parallel G-quadruplex appeared. These results indicated that **1** could induce the guanine-rich DNA to form the mixed parallel–antiparallel G-quadruplex structure. At the same time, a strong and positive induced CD signal was observed between 320 and 380 nm. This induced CD signal was additional evidence for the interaction between the G-quadruplex and complex **1**.[43]

The CD spectra of complex **2** titrated into the HTG21 oligonucleotide in the absence of salt was similar to, but not identical, that of complex **1** in the wavelength region below 300 nm. In Fig. 4b, it can be seen that titration of **2** into this DNA solution resulted in significant changes in the CD spectrum, including the observation of enhancement of the maximum at 290 nm and suppression of the band at 252 nm, shifting to 260 nm, and the emergence of a strong shoulder at 275 nm and a negative peak near 240 nm. The presence of these signals suggested that **2** can also induce the HTG21 to form the mixed parallel–antiparallel G-quadruplex structure.[44] It is worth noting that the shoulder near 275 nm induced by **2** is much more dramatical than that induced by **1**. The reason seems to be that the planar arrangement of the phen rings and

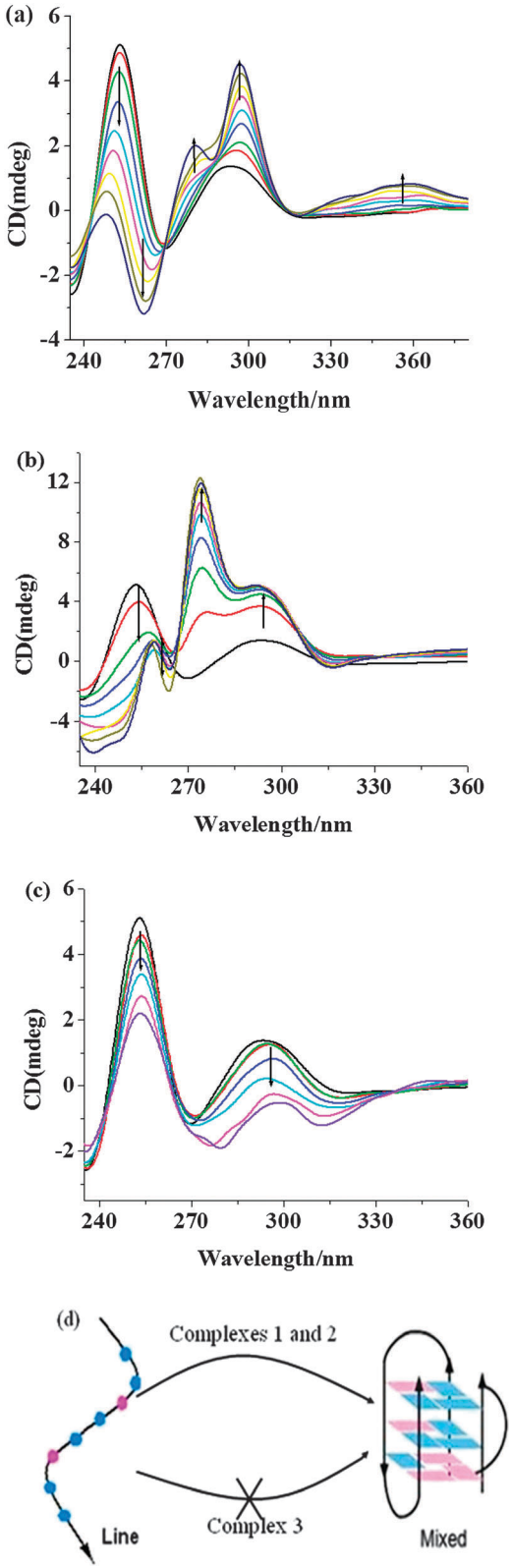

Fig. 4 CD spectra of the HTG21 in the presence of increasing amounts of complexes **1** (a), **2** (b) and **3** (c). [HTG21] = 2 μM, in 10 mM Tris-HCl, pH = 7.4, the complex concentration was 0–10 μM. (d) Illustration of how three ruthenium complexes induce single-stranded human telomeric DNA to form a mixed G-quadruplex.

Table 1 IC_{50} values (μM) of the complexes **1**, **2** and **3** after 48 h treatment in three selected cell lines

	IC_{50} (μM)		
Complexes	HeLa	A549	HepG2
1	89.4 ± 2.3	127 ± 1.5	103 ± 1.8
2	13.5 ± 0.5	19.2 ± 0.7	29.7 ± 0.6
3	67.2 ± 1.5	32.4 ± 0.9	59.1 ± 0.8
CDDP	7.6 ± 0.4	13.6 ± 0.3	26.8 ± 0.5

their appropriate spacing make **2** ideal to be stacked on top of the guanine tetrads.

In Fig. 4c, it can be seen that the bands at 252 and 292 nm greatly weaken with the addition of complex **3** into the same DNA solution, without the appearance of any new bands. The extraordinary result showed that complex **3** had no ability to induce the formation of mixed G-quadruplex structures. The spectral changes indicate that **1** and **2** can induce human telomeric DNA to form a mixed/hybrid type G-quadruplex structure (Fig. 4d).

3.5 *In vitro* cytotoxicity assay

In vitro cytotoxicity assay of complexes **1**, **2** and **3** was evaluated by means of MTT assay against three human cancer cell lines (using cisplatin as the positive control) including HeLa (human cervical cancer), A549 (human lung carcinoma) and HepG2 (human hepatocellular liver carcinoma).[45] After the cancer cells were incubated at various concentrations of tested complexes for 48 h, each complex exhibited different antitumor activities.

The IC_{50} values of three complexes and cisplatin are shown in Table 1. The results indicated that the cancer cells tested are susceptible to the complexes. As shown in Table 1, IC_{50} values of **1** on three cell lines range from 89.4 μM to 127 μM, which exhibited moderate cytotoxic activity. Compared to **1**, the IC_{50} value of **3** is lower, which shows that **3** is more active in the cell lines tested than **1**. It is interesting that complex **2** exhibited the highest antiproliferative activities in three cancer cell lines among the three complexes, as evidenced by the lowest IC_{50} values. Notably, **2** exhibited a broad spectrum of inhibition on human cancer cells, with IC_{50} values ranging from 13.5 to 29.7 μM, indicating the high cytotoxic effects of **2** on cancer cells. It is also worth noting that **2** shows a distinct preference for HeLa cells, thus HeLa cells were chosen as a cell model for further investigation of the mechanisms underlying the antiproliferative action of **2**.

To clarify how complex **2** affected HeLa cell growth, the changes in cell morphology were examined using an inverted microscope (Fig. 5A). We found that HeLa cells treated with complex **2** for 48 h exhibited marked morphologic signs of apoptosis in a dose-dependent manner, where lots of cells became round, detached cells increased and adherent cells gradually decreased, then a large number of suspended cells appeared, accompanied with cell debris, apoptotic bodies and other characteristics. To observe the morphologic characteristics of apoptotic nuclei, HeLa cells were stained with Hoechst 33342 after exposure to **2** (10 μM) and detected using

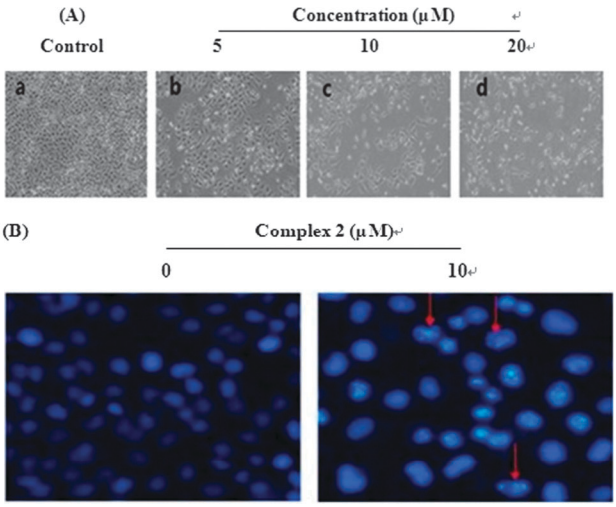

Fig. 5 Complex **2** induced apoptosis in HeLa cells. (A) The change of cell morphology observed using an inverted microscope (×200). Cells were treated with different concentrations of complex **2** for 48 h. (B) Complex **2** induced apoptotic morphological changes of HeLa cells. HeLa cells were treated with complex **2** for 48 h, stained with Hoechst 33342 and photographed using fluorescence microscopy (×400). The red arrows indicate the condensed or fragmented nucleus and multi-blebbing cells, respectively.

fluorescence microscopy. Apoptotic and necrotic cells can be distinguished from one another in fluorescence microscopy.[46] After treatment of HeLa cells with **2** for a period of 48 h, apoptotic bodies displaying different size and irregular morphology were observed as shown in Fig. 5B. However, staining bright, condensed chromatin and fragmented nuclei did not appear in the normal control group. The cells treated with **2** did exhibit morphologic features of apoptosis, and further quantitative analysis of changes in apoptosis is necessary.

3.6 TRAP assay

In order to examine the ability of the complexes to inhibit the telomerase activity, the telomeric repeat amplification protocol (TRAP) assay was performed.[47] Complexes **2** and **3** were tested in this experiment. Fig. 6 shows the *in vitro* inhibitory effect of **2** and **3**. The process of inhibition of telomerase activity was investigated in a dose-dependent manner, and the number of bands obviously decreased with respect to the control, in the drug concentration range of 1–20 μM. The two complexes tested

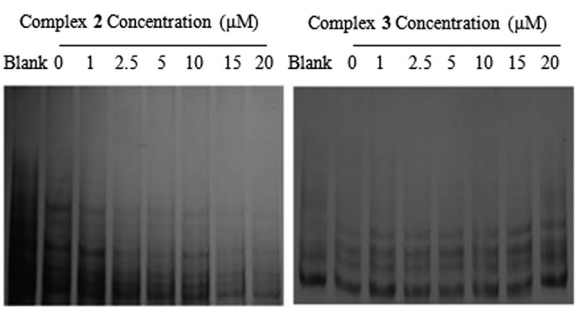

Fig. 6 The influence of complexes **2** and **3** on the telomere activity of HeLa cells.

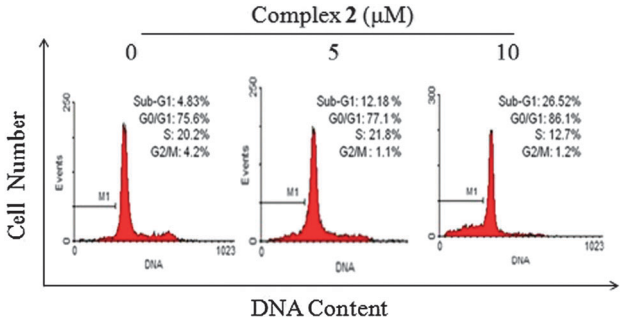

Fig. 7 Quantitative analysis of complex **2** induced apoptotic cell death (48 h) in HeLa cells using flow cytometry. The cells treated with different concentrations of complex **2** for 48 h were collected and stained with PI after fixation.

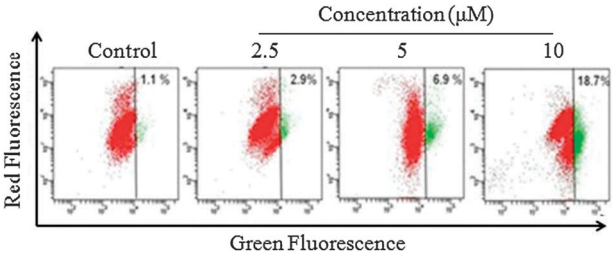

Fig. 8 Complex **2** induced the depletion of mitochondrial membrane potential ($\Delta\Psi_m$) in HeLa cells. Cells treated with different concentrations of complex **2** were analyzed using JC-1 flow cytometry. The number in each dot plot represents the percentage of cells that lost $\Delta\Psi_m$.

led to an inhibition of the telomerase activity, but there were differences in the extent of inhibition. Fig. 6 clearly revealed that **2** exhibited greater telomerase inhibitory activity than complex **3**. A number of methods have been previously used to confirm that complex **2** is a more effective stabilizer of HTG21, and shows stronger inhibition activity against cancer cells. According to all the above results, we can infer that telomerase is one of the targets for inhibiting tumors induced by the ruthenium complexes.

3.7 Cell cycle arrest and induction of apoptosis

The inhibition of cancer cell proliferation, the cessation of cell-cycle progression and the induction of apoptosis have all been targeted in chemotherapeutic strategies for the treatment of cancer.[48] We therefore evaluated whether complex **2** altered the cell cycle of HeLa cells and induced apoptosis of HeLa cells using flow cytometric analyses. The cell-cycle phase distribution in HeLa cells after 48 h exposure to different concentrations of **2** was analysed.

As shown in Fig. 7, treatment with **2** led to a marked dose-dependent increase in the proportion of cells in the G0/G1 phase. There were 77.1% and 86.1% cells in G0/G1 phase after 48 h treatment with **2** at concentrations of 5 and 10 μM, respectively, compared with 75.6% in untreated cultures; at the same time, the proportion of cells in the G2/M phase decreased significantly from 4.2% to 1.2%. This confirmed that the **2**-treated cells were blocked in the G0/G1-phase. The alteration of cells in the S phase after 48 h treatment with different concentrations of **2** was not regular. Furthermore, a population of sub-G1-phase cells, a characteristic of apoptosis, was increased dramatically with an increase in the concentration of **2**. These results indicated that cell death induced by complex **2** is mainly caused by induction of apoptosis.

3.8 Induction of mitochondrial dysfunction

Mitochondria control the life and death of a cell, deciding the fate of a cell by controlling the process of apoptosis.[49] Mitochondria act as a point of integration for apoptotic signals originating from both the extrinsic and intrinsic apoptotic pathways.[50] Mitochondrial dysfunction and the release of apoptogenic factors are critical keys in triggering various apoptotic pathways associated with the initiation of apoptotic cascades. Therefore, mitochondrial dysfunction was investigated by measuring changes in the mitochondrial membrane potential (MMP, $\Delta\Psi_m$) using flow cytometry after staining live cells with the cationic dye JC-1 (5,5′,6,6′-tetrachloro-1,1′,3,3′-tetraethylbenzimidazolylcarbocyanine iodide). JC-1 exhibits potential-dependent accumulation in mitochondria, indicated by a fluorescence emission shift from red to green. As depicted in Fig. 8, complex **2** significantly induced a dose-dependent decline of $\Delta\Psi_m$ in HeLa cells. The cell ratio of mitochondrial depolarization increased roughly by nearly 20 times, changing from 1.1% (control) to 2.9% (2.5 μM), then 6.9% (5 μM), finally up to 18.7% (10 μM). Its accumulation in HeLa cells then induced the loss of $\Delta\Psi_m$, led to the release of mitochondrial contents and apoptosis-related factors such as cytochrome *c* and other apoptosis-inducing factors, then DNA damage occurred and morphological changes appeared. The decline of $\Delta\Psi_m$ further confirmed that **2** induced apoptosis in HeLa cells through the endogenous mitochondria-mediated pathway.

4 Conclusions

In summary, three new ruthenium(II)-2,2′-bisimidazole complexes have been synthesized and made to interact with human telomeric G-quadruplex DNA. The experimental results implied that the three complexes could bind tightly to the human telomeric DNA. Complex **2** could significantly stabilize the G-quadruplex structure and exhibited more efficiency in inducing the formation of mixed/hybrid type G-quadruplexes compared to complexes **1** and **3**. This result might be explained by the fact that its auxiliary phen ligands are available for the π–π interactions between the aromatic phen ligands and DNA guanine residues, meanwhile, the great steric hindrance of the *p*-mopip ligands of complex **3** make them difficult to externally bind to the stacks of guanine quartets within a quadruplex or intercalating between the stacks. *In vitro* cytotoxicity assay data show that complex **2** exhibited more potent antitumor activities against cancer cell lines, compared to complexes **1** and **3**. This result showed that the antitumor activity is closely related to their ability to interact with G-quadruplex DNA, and complex **2** could effectively inhibit tumor cell growth. TRAP assay demonstrated that complex **2** exhibited stronger inhibitory

activity towards telomerase. Thus, the inhibition of telomerase activity by inducing G-quadruplex formation is very important for developing anticancer drugs. Complex **2** induced HeLa cells to generate a significant peak of apoptosis in the sub-G1 phase, indicating that complex **2** inhibits HeLa cells proliferation by induction of apoptosis. Further investigation showed that the treatment of the complex in HeLa cells could result in significant depletion of $\Delta\Psi_m$ in a dose-dependent manner, and it is a relatively early event in complex **2**-induced apoptosis. Taken together, these results demonstrated that complex **2** could effectively promote the apoptosis of tumor cells by acting on mitochondrial apoptotic pathways. The present results should be of value in further understanding the interaction of G-quadruplexes with metal complexes, as well as offer valuable information for designing new antitumor therapeutics.

Acknowledgements

This work was supported by the National Natural Science Foundation of China (20871056, 21171070, 21371075), the Planned Item of Science and Technology of Guangdong Province (c1011220800060, c1211220800571), the Natural Science Foundation of Guangdong Province and the Fundamental Research Funds for the Central Universities.

Notes and references

1 N. W. Kim, M. A. Piatyszek, K. R. Prowse, C. B. Harley, M. D. West, P. L. Ho, G. M. Coviello, W. E. Wright, S. L. Weinrich and J. W. Shay, *Science*, 1994, **266**, 2011–2015.
2 J. Szolomájer, G. Paragi, G. Batta, C. F. Guerra, F. M. Bickelhaupt, Z. Kele, P. Pádár, Z. Kupihár and L. Kovács, *New J. Chem.*, 2011, **35**, 476–482.
3 C. C. Chang, I. C. Kuo, I. F. Ling, C. T. Chen, H. C. Chen, P. J. Lou, J. J. Lin and T. C. Chang, *Anal. Chem.*, 2004, **76**, 4490–4494.
4 K. Paeschke, S. Juranek, D. Rhodes and H. J. Lipps, *Chromosome Res.*, 2008, **16**, 721–728.
5 A. Paul, B. Maji, S. K. Misra, A. K. Jain, K. Muniyappa and S. Bhattacharya, *J. Med. Chem.*, 2012, **55**, 7460–7471.
6 A. M. Burger, F. Dai, C. M. Schultes, A. P. Reszka, M. J. Moore, J. A. Double and S. Neidle, *Cancer Res.*, 2005, **65**, 1489–1496.
7 Y.-P. Huang, D.-M. Kong, Q.-M. Chen, H.-X. Shen and H.-F. Mi, *New J. Chem.*, 2004, **28**, 1488–1493.
8 K. Masutomi, E. Y. Yu, S. Khurts, I. Ben-Porath, J. L. Currier, G. B. Metz, M. W. Brooks, S. Kaneko, S. Murakami, J. A. DeCaprio, R. A. Weinberg, S. A. Stewart and W. C. Hahn, *Cell*, 2003, **114**, 241–253.
9 C. Zhao, J. Geng, L. Feng, J. Ren and X. Qu, *Chem.–Eur. J.*, 2011, **17**, 8209–8215.
10 S. N. Georgiades, N. H. Abd Karim, K. Suntharalingam and R. Vilar, *Angew. Chem., Int. Ed.*, 2010, **49**, 4020–4034.
11 J. E. Reed, S. Neidle and R. Vilar, *Chem. Commun.*, 2007, 4366–4368.
12 J. E. Reed, A. A. Arnal, S. Neidle and R. Vilar, *J. Am. Chem. Soc.*, 2006, **128**, 5992–5993.
13 N. V. Anantha, M. Azam and R. D. Sheardy, *Biochemistry*, 1998, **37**, 2709–2714.
14 H. Yu, X. Wang, M. Fu, J. Ren and X. Qu, *Nucleic Acids Res.*, 2008, **36**, 5695–5703.
15 B. M. Zeglis, V. C. Pierre and J. K. Barton, *Chem. Commun.*, 2007, 4565–4579.
16 M. R. Gill and J. A. Thomas, *Chem. Soc. Rev.*, 2012, **41**, 3179–3192.
17 H. Song, J. T. Kaiser and J. K. Barton, *Nat. Chem.*, 2012, **4**, 615–620.
18 G. N. Parkinson, M. P. Lee and S. Neidle, *Nature*, 2002, **417**, 876–880.
19 K. E. Erkkila, D. T. Odom and J. K. Barton, *Chem. Rev.*, 1999, **99**, 2777–2796.
20 C. Metcalfe and J. A. Thomas, *Chem. Soc. Rev.*, 2003, **32**, 215–224.
21 U. Schatzschneider, J. Niesel, I. Ott, R. Gust, H. Alborzinia and S. Wölfl, *ChemMedChem*, 2008, **3**, 1104–1109.
22 S. Rickling, L. Ghisdavu, F. Pierard, P. Gerbaux, M. Surin, P. Murat, E. Defrancq, C. Moucheron and A. Kirsch-De Mesmaeker, *Chem.–Eur. J.*, 2010, **16**, 3951–3961.
23 C. Rajput, R. Rutkaite, L. Swanson, I. Haq and J. A. Thomas, *Chem.–Eur. J.*, 2006, **12**, 4611–4619.
24 F. Linares, M. A. Galindo, S. Galli, M. A. Romero, J. A. Navarro and E. Barea, *Inorg. Chem.*, 2009, **48**, 7413–7420.
25 O. Zava, S. M. Zakeeruddin, C. Danelon, H. Vogel, M. Gratzel and P. J. Dyson, *ChemBioChem*, 2009, **10**, 1796–1800.
26 J. M. Rademaker-Lakhai, D. van den Bongard, D. Pluim, J. H. Beijnen and J. H. Schellens, *Clin. Cancer Res.*, 2004, **10**, 3717–3727.
27 F. Barragan, D. Carrion-Salip, I. Gomez-Pinto, A. Gonzalez-Canto, P. J. Sadler, R. de Llorens, V. Moreno, C. Gonzalez, A. Massaguer and V. Marchan, *Bioconjugate Chem.*, 2012, **23**, 1838–1855.
28 V. Pierroz, T. Joshi, A. Leonidova, C. Mari, J. Schur, I. Ott, L. Spiccia, S. Ferrari and G. Gasser, *J. Am. Chem. Soc.*, 2012, **134**, 20376–20387.
29 I. Ascone, L. Messori, A. Casini, C. Gabbiani, A. Balerna, F. Dell'Unto and A. C. Castellano, *Inorg. Chem.*, 2008, **47**, 8629–8634.
30 M. Groessl, E. Reisner, C. G. Hartinger, R. Eichinger, O. Semenova, A. R. Timerbaev, M. A. Jakupec, V. B. Arion and B. K. Keppler, *J. Med. Chem.*, 2007, **50**, 2185–2193.
31 D. Sun, Y. Liu, D. Liu, R. Zhang, X. Yang and J. Liu, *Chem.–Eur. J.*, 2012, **18**, 4285–4295.
32 S. Shi, J. Liu, J. Li, K. C. Zheng, X. M. Huang, C. P. Tan, L. M. Chen and L. N. Ji, *J. Inorg. Biochem.*, 2006, **100**, 385–395.
33 J. Bolger, A. Gourdon, E. Ishow and J. P. Launay, *Inorg. Chem.*, 1996, **35**, 2937–2944.
34 W. Paw and R. Eisenberg, *Inorg. Chem.*, 1997, **36**, 2287–2293.
35 J. C. Xiao and J. M. Shreeve, *J. Org. Chem.*, 2005, **70**, 3072–3078.
36 Z.-C. Liu, B.-D. Wang, Z.-Y. Yang, Y. Li, D.-D. Qin and T.-R. Li, *Eur. J. Med. Chem.*, 2009, **44**, 4477–4484.

37 A. Tarushi, J. Kljun, I. Turel, A. A. Pantazaki, G. Psomas and D. P. Kessissoglou, *New J. Chem.*, 2013, **37**, 342–355.
38 S. Cogoi, M. Paramasivam, B. Spolaore and L. E. Xodo, *Nucleic Acids Res.*, 2008, **36**, 3765–8010.
39 D. Sun, R. Zhang, F. Yuan, D. Liu, Y. Zhou and J. Liu, *Dalton Trans.*, 2012, **41**, 1734–1741.
40 E. M. Rezler, J. Seenisamy, S. Bashyam, M. Y. Kim, E. White, W. D. Wilson and L. H. Hurley, *J. Am. Chem. Soc.*, 2005, **127**, 9439–9447.
41 R. Rodriguez, G. D. Pantos, D. P. Goncalves, J. K. Sanders and S. Balasubramanian, *Angew. Chem., Int. Ed.*, 2007, **46**, 5405–5407.
42 J. L. Mergny and J. C. Maurizot, *ChemBioChem*, 2001, **2**, 124–132.
43 E. W. White, F. Tanious, M. A. Ismail, A. P. Reszka, S. Neidle, D. W. Boykin and W. D. Wilson, *Biophys. Chem.*, 2007, **126**, 140–153.
44 Y. Xu, Y. Noguchi and H. Sugiyama, *Bioorg. Med. Chem.*, 2006, **14**, 5584–5591.
45 X. Zhang, X. Li, S. Ye, Y. Zhang, L. Tao, Y. Gao, D. Gong, M. Xi, H. Meng, M. Zhang, W. Gao, X. Xu, Q. Guo and Q. You, *Med. Chem.*, 2012, **8**, 1012–1025.
46 M. Takaya, M. Nomura, T. Takahashi, Y. Kondo, K. T. Lee and S. Kobayashi, *Anticancer Res.*, 2009, **29**, 995–1000.
47 X. Chen, J. H. Wu, Y. W. Lai, R. Zhao, H. Chao and L. N. Ji, *Dalton Trans.*, 2013, **42**, 4386–4397.
48 Y. Jin, J. Liu, W.-T. Huang, S.-W. Chen and L. Hui, *Eur. J. Med. Chem.*, 2011, **46**, 4056–4061.
49 X. Yang, L. Chen, Y. Liu, Y. Yang, T. Chen, W. Zheng, J. Liu and Q. Y. He, *Biochimie*, 2012, **94**, 345–353.
50 C. A. Puckett, R. J. Ernst and J. K. Barton, *Dalton Trans.*, 2010, **39**, 1159–1170.

